THE ASTROPHYSICAL JOURNAL, 271:335–354, 1983 August 1

DETERMINATION OF THE SOLAR WIND ANGULAR MOMENTUM FLUX FROM THE *HELIOS* DATA—AN OBSERVATIONAL TEST OF THE WEBER AND DAVIS THEORY

V. PIZZO
High Altitude Observatory, National Center for Atmospheric Research[1]
R. SCHWENN, E. MARSCH, AND H. ROSENBAUER
Max-Planck-Institut für Aeronomie
K.-H. MÜHLHÄUSER
Max-Planck-Institut für Physik und Astrophysik
AND
F. M. NEUBAUER[2]
Institut für Geophysik und Meteorologie der Technische Universitat zu Braunschweig
Received 1982 December 13; accepted 1983 January 24

ABSTRACT

In situ attempts to measure the sun's angular momentum loss in the solar wind and thereby to test the Weber and Davis description of the magnetic coupling between stellar rotation and winds have thus far produced widely divergent and inconclusive results. A new estimate for the solar loss rate in the ecliptic plane has been derived from the *Helios* spacecraft data. By intercomparing measurements made by the twin probes over the full 0.3–1.0 AU baseline of their orbits, it is possible to eliminate the systematic instrumental offsets from the true radial direction that have plagued previous efforts. The main observational findings are that (1) the total angular momentum flux loss rate (field + particles) near the solar equator is ~ 0.2–0.3×10^{30} dyn cm sr^{-1}, about one-quarter the Weber and Davis prediction and much lower than previous spacecraft estimates, and (2) the distribution of that flux between particles and field stresses is very near the 1:3 ratio of the model, when an important contribution from the heretofore neglected solar wind α-particles is accounted for. Though few by number in the solar wind, the α-particles' flow speed and direction in general differ from that of the protons, largely offsetting the latters' angular momentum content ($+0.15$–0.2×10^{30} for the protons, -0.1×10^{30} for the α-particles, plus being in the direction of corotation with the Sun). As to the small value reported for the total flux, theory and observation can be reconciled by moving the mean Alfvén radius, r_A, in to 12 $R_\odot$, a figure that is consistent with coronal models more realistic than the single polytrope formulation used by Weber and Davis. There is a distinct tendency for slow solar wind to carry positive total flux and for fast wind, negative; this can probably be explained in terms of stream-interaction dynamics in the super-Alfvénic region. It thus appears that the Weber and Davis theory adequately describes angular momentum loss in solar-type winds, insofar as simple magnetic stresses are taken as the dominant coupling mechanism. However, in the general astrophysical application, it is suggested that a more accurate treatment of coronal acceleration be incorporated to properly locate r_A (and hence fix the total loss rate) and that some allowance for three-dimensional effects be made. Also, should large speed differentials between α-particles and protons occur well inside r_A, a three-fluid version of the Weber and Davis model may be in order.

Subject headings: Sun: corona — Sun: rotation — Sun: solar wind

I. INTRODUCTION

The subject of the solar angular momentum lost in the solar wind expansion has been a source of frustration to theorists and experimenters alike for many years. While it is easy to obtain crude order-of-magnitude estimates of the present-day flux loss on the basis of simple physical arguments (Parker 1958; Dicke 1964), it has proven exceedingly difficult to secure a more detailed understanding of the phenomenon with any degree of certitude.

Early theoretical work on the subject was directed at assessing the effects of magnetic stresses in the corona, which are evidently the prime factor in coupling solar rotation with the azimuthal motion of the solar wind (Pneuman 1966; Modisette 1967; Alfonso-Faus 1968; Ferraro and Bhatia 1967; Mestel 1968; Weber 1969). The landmark paper in the field was by Weber and Davis (1967), who were the first to succeed in solving

[1] The National Center for Atmospheric Research is sponsored by the National Science Foundation.

[2] New address: Institut für Geophysik und Meteorologie der Universitat zu Köln, 5000 Köln-41 Federal Republic of Germany.

self-consistently the mass, radial momentum, and azimuthal momentum equations for axisymmetric, polytropic, single-fluid flow in the equatorial plane. Among the primary findings of their investigation were the predictions that the solar wind azimuthal flow velocity, u_ϕ, in interplanetary space should be very small (~ 1 km s^{-1} near 1 AU) and that most of the angular momentum flux (about three-fourths of the total, which is on the order of 10^{30} dyne-cm sr^{-1} in the model) should reside in the magnetic stresses.

These predictions have been viewed as being at variance with the observations then available and have remained so to this day. Estimates of the solar wind azimuthal speed garnered from comet tail data indicated an average velocity on the order of 9 km s^{-1} (Brandt 1967; Brandt and Heise 1970), while the first few direct measurements of solar wind direction showed an average flow angle at 1 AU of, variously, $+1\overset{\circ}{.}4$ (*Vela 2*, Strong *et al.* 1967), $+2\overset{\circ}{.}52$ and $+0\overset{\circ}{.}93$ (*Vela 3A-B*, Hundhausen *et al.* 1970), $-1\overset{\circ}{.}5$ (*Explorer 18*, Egidi, Pizella, and Signorini 1969), and $-3\overset{\circ}{.}0$ and $-0\overset{\circ}{.}31$ (*Pioneer 6–7*, Wolfe 1972). (Here a plus sign indicates flow in the direction of solar rotation.) The positive values quoted above imply a much larger azimuthal velocity component than predicted by theory, assuming "average" densities and radial speeds. Hardorp's (1971) analysis of *Vela 3* angular momentum flux densities was consistent with the interpretations of the *Vela 3* flow angles and corroborated the view that most of the flux is carried by the particles. Finally, Lazarus and Goldstein (1971) reported a determination of both particle and magnetic angular momentum flux based upon measurements taken by *Mariner 5*. Their findings were in agreement with theory in terms of total angular momentum flux ($\sim 10^{30}$ dyn-cm sr^{-1} near the ecliptic plane), but their results, too, indicated that the dominant contribution comes from the particles instead of the field.

Despite the wide range of reported observational values, the suspicion that something important was lacking in the basic Weber and Davis model spurred numerous theoretical efforts to find additional physical mechanisms capable of resolving the apparent discrepancy (e.g., increasing the 1 AU azimuthal flow speed to ~ 10 km s^{-1}). Schubert and Coleman (1968) suggested that compressive MHD waves in the interplanetary medium might tend to equalize the magnetic and particle flux contributions. Brandt, Wolff, and Cassinelli (1969) investigated the consequences of dispensing with the polytropic assumption and solved the single-fluid equations with field-inhibited Spitzer conduction taken into account. For the same boundary conditions as used by Weber and Davis (1967), they were able to increase the 1 AU u_ϕ up to ~ 2.5 km s^{-1}. Urch (1969) found similar results (1–2 km s^{-1}) for somewhat different boundary conditions. Weber (1970) considered the effects of thermal anisotropy, showing that for specified radial profiles of the radial velocity, density, and pressure anisotropy, u_ϕ could be raised to 3 km s^{-1} at 1 AU. A more detailed study of thermal anisotropy and field-inhibited viscosity, wherein only the radial velocity profile was specified, yielded a value of $u_\phi \approx 6$ km s^{-1} (Weber and Davis 1970). However, Wolff, Brandt, and Southwick (1971) noted that when a two-fluid description was employed, u_ϕ dropped back to ~ 2.5 km s^{-1}, by virtue of the more accurate treatment of the proton temperature radial profile. Hollweg (1973) showed that single-fluid non-WKB Alfvén waves were likely to decrease u_ϕ slightly from the Weber and Davis (1967) values, mainly by lowering the Alfvénic critical point. Finally, Acuña and Whang (1976) found $u_\phi < 2$ km s^{-1} in a mixed one-fluid, two-fluid model that incorporated inhibited conduction but no viscosity.

What to make of all this—both theory and observation—is not immediately obvious, and the entire topic has languished in confusion for a decade (e.g., see the panel discussion in *Solar Wind* 1972 and comments in Hundhausen 1972). Clearly, if any order is to be brought to the situation, the impetus must necessarily come from the observational side.

The store of data collected by the twin *Helios* probes affords just such an opportunity. These two essentially identical spacecraft were launched just prior to solar minimum, penetrating in elliptical orbits to within ~ 0.3 AU of the Sun. Judicious cross-analysis of the data returned by *Helios* makes it possible to ferret out spurious systematic effects that have plagued previous spacecraft measurements and thereby to derive the first reliable values for the solar angular momentum flux loss near the ecliptic plane.

Section II begins with a discussion of general physical considerations pertinent to the measurement of the angular momentum content of the solar wind by spacecraft. Section III follows with a review of empirical sources of systematic bias that can adversely affect the results. Section IV takes a careful look at an important subset of the *Helios* data, that obtained during the primary mission of each spacecraft. It describes an analysis that removes the systematic errors and yields a corrected evaluation of the solar wind angular momentum flux transport. Section V contains supplementary analysis of a much broader portion of the data, and § VI summarizes the basic results. Our best estimate for the magnitude of the average angular momentum flux loss is much smaller than (about one-quarter) previous theoretical and observational values and suggests a more realistic location for the mean coronal Alfvén radius might be near 12 $R_\odot$. Our results differ sharply from earlier observational assessments of the relative distribution of angular momentum flux between particles and field. Our findings, which include the first measurement of an important contribution from the α-particles, indicate that the angular momentum flux borne by the particles (protons plus alphas) is somewhat less than that in the magnetic stresses, in rough accord with the original Weber and Davis (1967) model. When corrected for the location of the Alfvén radius, then, the basic theory of magnetic coupling appears to adequately describe the nature of

angular momentum transport in the solar wind without any additional physical mechanisms heuristically invoked to increase u_ϕ near 1 AU. Finally, § VII closes with a discussion of the implications of these results for solar and stellar astrophysics.

II. FUNDAMENTAL CONSIDERATIONS

The primary constituents of the interplanetary plasma are electrons, protons, and helium, in order of numerical abundance. By taking the standard moments of the kinetic equations for each of these three species and summing, it is possible to derive the following time and longitudinally averaged conservation law for solar wind angular momentum flux near the ecliptic plane:

$$F \equiv r^3 \left[(\rho u_r u_\phi)_p + (\rho u_r u_\phi)_\alpha - \frac{B_r B_\phi}{4\pi} + (\cdots) \right] = \text{constant} . \quad (1)$$

Here F is the specific angular momentum loss rate (torque per steradian), r the heliocentric radius, ϕ the azimuthal coordinate in a spherical system (+ in the direction of corotation), $u_{r,\phi}$ the velocity components, $B_{r,\phi}$ the field components, and ρ the mass density, with subscripts p and α referring to protons and alphas. The first three terms represent the mechanical flux in the protons and alphas and the flux in the magnetic stresses, respectively. The ellipsis is a catchall for such lesser contributions to the total, such as electron mechanical flux, thermal anisotropies, time-averaged wave angular momentum flux, etc., which are presumably negligible beyond 0.3 AU. By actual measurement with the *Helios* data, the average thermal anisotropy about the species mean velocity, which would enter as $r^3 P_{r\phi}$ in (1), proves at least two orders of magnitude smaller than the other terms and will therefore be discussed no further. Wave contributions have not been specifically evaluated, but there is little reason to expect Alfvén waves to have a sizable net impact in interplanetary space (Hollweg 1973), nor do the amplitudes of compressive MHD waves in the solar wind appear to be large enough (Neugebauer, Wu, and Huba 1978) to make the mechanism of Schubert and Coleman (1968) important. Geometric source terms do appear on the right-hand side of (1) off the equator, but these should be very small in the vicinity of the ecliptic. Of more concern might be large scale systematic convergence/divergence of material into/out of the plane of observation by interplanetary dynamic processes. Axisymmetric MHD models show only a small effect (Nerney and Suess 1975), but a three-dimensional (3D) MHD model does suggest that the meridional transport of angular momentum by corotating streams could be significant in certain situations (Pizzo 1982). The only way to unequivocally identify such effects, however, would be to obtain measurements over a much larger range of latitudes than those sampled by *Helios*.

The alpha contribution in (1) requires special attention. Despite their low relative abundance, the helium ions nevertheless carry about 20% of the linear momentum in the solar wind. Furthermore, their speeds, flow directions, and subsequently their angular momentum content can differ substantially from that of the protons. It has been experimentally verified that when proton and alpha speeds are not equal, the difference vector tends to lie along $\boldsymbol{B}$ (Asbridge *et al.* 1976; Marsch *et al.* 1981, 1982*a*). Figure 1 shows the orientation of the flow vectors for a typical quasi-steady high-speed stream situation. Inasmuch as proton and alpha speeds can differ by as much as 150 km s^{-1} in streams, it is evident that the angular momentum content of the α-particles must be separately measured in any serious study of angular momentum flux loss from the Sun.

Spacecraft observations unavoidably mix spatial and temporal variations, so that strictly speaking it is not possible to form the pure average (1). This effect could prove particularly vexing for longer period variations (on the order of a few rotations) since *Helios* can move large distances in radius and solar latitude in that length of time. On the short time-scale end, *Helios* provides no information on angular momentum flux variations more rapid than the 40 s temporal resolution of the plasma instruments. Between these two extremes, the main sources of the observed variations are Alfvén waves of several minutes period, quasi-steady corotating streams, and large-scale impulsive flows associated with coronal transients. Hence accurate determination of the mean F is contingent upon collecting measurements across many flow states.

It is useful to inquire just how much transients are likely to influence angular momentum transport in the solar wind. A rough estimate of the global effects can be obtained by comparing the expected angular momentum loss of quasi-steady origin summed over a solar rotation with that anticipated from a single large solar flare ejection. For the sake of argument, let us use a figure of $F = 10^{30}$ dyne-cm sr^{-1} as the mean specific angular momentum flux at the equator (Lazarus

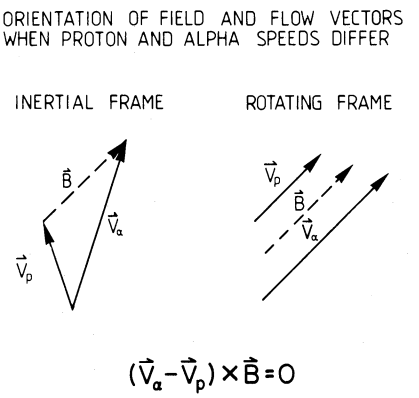

FIG. 1.—The difference vector between alpha and proton velocities normally lies along the magnetic field. For the steady flow situation shown, all three vectors are parallel in a frame rotating with the Sun. In the inertial frame the alpha and proton flow angles can differ appreciably.

and Goldstein 1971). Assuming a $\sin\theta$ dependence for F, the global quasi-steady angular momentum loss from the Sun in one rotation is

$$10^{30} \times \iint \sin^2\theta d\theta d\phi \times 25.4 \times 8.64 \times 10^4 \approx 2 \times 10^{37} \text{ dyn-cm-s}$$

Now consider a worst-case flare, a large eruption in which all ejecta are blasted free from the Sun tangent to the surface along the equator. Assuming a total ejected mass of $M = 10^{17}$ g (Hundhausen, Bame, and Montgomery 1970) and a speed of $V = 1000$ km s^{-1}, the angular momentum lost/gained in the flare is

$$MVR_\odot \approx 7 \times 10^{35} \text{ dyn-cm-s} .$$

Thus about 30 such worst-case eruptions per solar rotation (all in the same direction) would be required to match the quasi-steady component. We therefore conclude that transients should contribute little to the solar wind angular momentum loss globally. Nevertheless, they can cause sizable local fluctuations in the specific angular momentum flux (cf. Fig. 4), and it is therefore fortunate that they occur rarely, at least in the primary mission data.

III. EMPIRICAL CONSTRAINTS

Because the Sun is a slowly rotating star with relatively weak magnetic fields, the angular momentum flux whisked away in the solar wind is exceedingly small. This tenuous transport is, furthermore, subject to systematic and random variations that can be orders of magnitude larger than the mean. Consequently, the accurate determination of the solar wind angular momentum flux presents an extraordinary experimental challenge. In this section we will examine those aspects of the *Helios* instrumentation and data reduction procedures which bear upon our ability to measure this elusive quantity.

a) The Root of the Observational Problem

From the standpoint of angular momentum observations, there are two main empirical problems to be overcome. The first is simply that the fluctuations in F can be orders of magnitude larger than the average. The second is that the radial momentum flux density in the protons is many, many times larger than the tangential components, i.e., the flow is very nearly radial. What this means is that for any given individual spectra, even a slight error in the determination of the azimuthal flow direction translates into a large error in angular momentum flux. To see how this comes about, consider that the proton specific angular momentum flux

$$F_p = r^3 \rho u_r u_\phi$$

can be rewritten

$$r(r^2\rho u_r^2)\left(\frac{u_\phi}{u_r}\right) = r(r^2\rho u_r^2)\tan\phi . \quad (2)$$

For some small inaccuracy $\delta\phi$ in the determination of ϕ, the error in F_p is, approximately,

$$\delta F_p = r(r^2\rho u_r^2)\delta\phi . \quad (3)$$

The term in the parentheses is none other than the radial mechanical momentum flux, which is only weakly dependent upon radius in the interplanetary region. Thus, should some bias $\delta\phi$ creep into the data acquisition, a radially dependent trend will be impressed upon the measurements. Conversely, any systematic error linearly dependent on radius will affect the data like a small-angle rotational misalignment of the coordinate axes.

To get an idea of the magnitude of this error for a typical 400 km s^{-1}, 7 proton cm^{-3} solar wind at 1 AU, equation (3) yields, approximately,

$$\delta F_p \approx r[\text{AU}]\delta\phi[\text{deg}] \times 10^{30} \text{ dyn-cm sr}^{-1} . \quad (4)$$

That is, at 1 AU an offset of 1° produces an error as large as the nominal Lazarus and Goldstein (1971) value ($\sim 10^{30}$ dyn-cm sr^{-1}) for the specific solar wind angular momentum flux. For reference, this relation can also be expressed in terms of a spurious azimuthal velocity component, δu_ϕ:

$$\delta F_p \approx r[\text{AU}]\delta u_\phi[\text{km s}^{-1}] \times 1.6 \times 10^{29} \text{ dyn-cm sr}^{-1} . \quad (5)$$

While similar arguments can be extended to the determination of the alpha flux F_α (with the further complication of lower counting rates and statistical accuracy), the prospects for obtaining a reliable estimate of the magnetic stress contribution to F are much brighter. The reason is simply that the field is not so radially directed on average as the flow, and hence the magnetic specific flux

$$F_B = -r^3(B_r B_\phi/4\pi)$$

is relatively insensitive to small errors in the magnetic field components. For comparison with (4), a directional error $\delta\phi$ leads to

$$\delta F_B \approx \frac{(r^2 B_r)^2}{4\pi}\frac{\delta\phi}{r} \approx \frac{\delta\phi(\text{deg})}{r[\text{AU}]} \times 7 \times 10^{27} \text{ dyn-cm sr}^{-1} \quad (6)$$

for $B_r(1 \text{ AU}) = 4\gamma$ and $r^2 B_r \approx$ const by virtue of $\nabla \cdot \boldsymbol{B} = 0$. Particularly near 1 AU, then, it is safe to discount orientation errors insofar as the field is concerned. However, there is an additional problem with the field measurements associated with corrections to account for the combined effects of sensor zero-offsets and spacecraft magnetic field. Fortunately, these are of the order of 10% or less and have little impact upon our final results.

b) Synopsis of the Helios Instrumentation

For those concerned primarily with the physical insights to be gained from study of the *Helios* data, a laborious recounting of instrumental minutiae may

be most unwelcome. However, just such details, which can normally be accorded only the most cursory attention, are crucial to assessing the validity of the observed angular momentum flux and cannot be legitimately avoided. Consequently, this subsection will be devoted to a brief overview of the *Helios* instruments involved in this effort, and the next will discuss aspects of instrumentation and data analysis specifically related to angular momentum measurements. Further details not covered here can be found in Schwenn, Rosenbauer, and Miggenrieder (1975), Rosenbauer *et al.* (1977), Marsch *et al.* (1982*b*), and Neubauer *et al.* (1977). (For reference, Strong *et al.* [unpublished manuscript] delve into similar practical topics in their analysis of *Vela 3* data.)

The *Helios* mission involves two virtually identical spacecraft placed in Sun-centered elliptical orbits having perihelia of about 0.3 AU and aphelia near 1.0 AU. These spacecraft were carefully engineered to reduce magnetic and electric field contamination to a minimum, and the mechanical and electrical operation of the instruments was painstakingly calibrated to facilitate measurements of the very quantities in which we are interested. The magnetic instruments are located at the ends of special booms projecting out several meters from the drum-shaped, heat-insulated spacecraft bus. All magnetic field data used here are from the experiment of the Technical University of Braunschweig (Musmann *et al.* 1975), with components averaged over the 40 s period of the plasma spectra. The two plasma instruments relevant to this study are internally mounted in the spacecraft bus. The primary instrument, I1a, uses continuous electron multipliers (CEMs) to count particles sorted according to energy per charge by a quadrispheric electrostatic deflector. Nine CEMs provide directional resolution in spacecraft polar angle (θ), while directional resolution in azimuth (ϕ) is obtained by making use of the spacecraft spin. Every rotation period (which is 1 s), the electrostatic deflector is stepped to a new energy level until all 32 energy channels are monitored. In this manner a full 3D spectrum is assembled every 40 s. When the spacecraft are near the Sun ($r < 0.6$ AU) and the solar wind mass flux is high, the mass spectrometer I3 can be employed instead. This instrument operates similarly to I1a, its chief function being to screen out the alphas so that an uncontaminated proton distribution function can be obtained.

c) Systematic Error of Instrumental Origin

As was pointed out above, systematic errors of even a few kilometers per second in determination of the azimuthal velocity prove intolerable. Therefore, in this subsection we discuss the two main sources of instrumental error—viz., pointing inaccuracy and spacecraft charging.

We first call attention to the fact that *Helios* derives its azimuthal resolution from the spacecraft spin and that the Sun sensor is not integral to the plasma instrument itself. Rather, determination of the instantaneous look direction hinges upon timing pulses delivered by an external sensor. Though the tolerances on machining and laboratory calibration of the mechanical alignment between sensor and plasma instrument were less than 0°.1, thermal warps affecting pointing accuracy might be encountered, as noted in other spacecraft (A. Skumanich, private communication). The magnetic experiments, being suspended on booms, are also susceptible to flexture problems, but, as shown above, small directional errors in the magnetic component are inconsequential. Fortunately, the only worrisome pointing errors are those corresponding to a simple coordinate rotation in the r-ϕ plane, i.e., rotation about the spacecraft polar axis. Rotations about the other two axes cause some small fraction of the θ-momentum to appear in the ϕ-direction. But since both nonradial momenta are generally of the same order, on average this amounts to a correction of only a few percent in either component, which is far, far less than any of the other uncertainties we have to confront. On this basis, it is unnecessary to transform the data from the Sun-centered ecliptic coordinates used in the routine survey publications to heliographic coordinates, nor is directional resolution in the θ-coordinate important in measuring the azimuthal momentum flux.

Electric charging of the spacecraft poses more serious problems. Of particular concern is the possibility of asymmetric charging, whose effects cannot be adequately assessed. For example, weak azimuthal electric fields could be set up as the quartz surfaces of the spacecraft change their potential in passing between sunward and shadowed sectors of the spinning spacecraft (Könemann and Schröder 1974). The resultant deflection of the incoming beam might be negligible by ordinary standards, but in view of the extreme accuracy required for the angular momentum determination such charging effects cannot be casually dismissed.

Systematic errors due to both pointing and charging effects could be completely avoided if either the plasma instruments or the entire spacecraft could be flipped over frequently (cf. Lazarus and Goldstein 1971). Unfortunately, practical difficulties prevented implementation of this scheme for *Helios*, so the next best alternative was adopted. The orientations of *Helios A* and *B* were inverted at launch, with the sense of *Helios A*'s spin being the same as the Sun's. The idea was that essentially identical spacecraft spinning upside down relative to each other should produce equal and opposite biases in the data and the systematic error, whatever its origin, could thereby be removed. This foresight proves crucial in the development of our analysis.

d) Systematic Bias in the Data Reduction Methods

The reduction of the raw spectra can also introduce systematic bias into the determination of the angular momentum flux. The 3D spectra from both plasma instruments are analyzed in two distinct ways. The simpler method (Rosenbauer *et al.* 1977), used for the routine survey of all positive ion data, synthesizes a

3D analysis from three reduced distributions in the angles ϕ and θ and bulk speed, v. The reduced distribution for any one of these variables is obtained by summations over the other two, and hence the technique is referred to as the 1D analysis. The bulk proton velocity vector, density, and the temperature in three directions result from the analysis, as well as estimates of the alpha bulk speed (but no directional information), density, and temperature. The 1D technique offers the advantage of numerical efficiency, so that a great deal of data can be rapidly analyzed. The other method is a full 3D moments analysis (Marsch *et al.* 1982*b*) which allows a much more complete description of the plasma. Velocity vector, density, thermal tensor, and heat flux vector are all determined for both protons and alphas, along with other useful plasma quantities. Unfortunately, the 3D moments method is computationally expensive and can therefore be applied only sparingly to the data. Since the two techniques yield slightly different results, both reductions are utilized in the analysis. While there are some visible discrepancies between the two (discussed at length in § V*b*), the basic interpretation of our results is not compromised. Indeed, we develop the analysis by concentrating first on the highly detailed but limited number of 3D moments data from the primary mission, then using the much larger volume of 1D data to cross-check the two reductions and to improve upon the statistics.

IV. ANALYSIS OF THE PRIMARY MISSION DATA BY THE 3D MOMENTS METHOD

In this section, we present an analysis of an important subset of the *Helios* accumulation, the primary mission data (first perihelion passage of each spacecraft). We discuss important general aspect of the observations, including how the angular momentum flux is distributed relative to the dominant solar wind structures of the period, the quasi-steady interacting streams. Finally, we eliminate a systematic offset in the measured angular momentum flux between the two spacecraft and obtain corrected estimates for the total and constituent solar wind angular momentum fluxes.

a) Helios Data Used in This Part of the Analysis

The only portion of the *Helios* data presently available that offers a sufficient span of relatively continuous sampling with the 3D decomposition comes from the primary mission period of each spacecraft. For *Helios A*, we will be using 7910 plasma spectra collected between 1974 December 13 and 1975 April 6. These data cover the second half of Carrington rotation (CR) 1621 and nearly all of three following rotations in CR 1622–1625. For *Helios B*, there are 7700 data points obtained from 1976 January 17 to 1976 May 9, covering slightly more than three solar rotations between CR 1636 and 1641. In each sequence, the spacecraft spends most of its time at negative heliocentric latitudes near 1 AU, then sweeps rapidly through perihelion, crossing over into the northern solar hemisphere at the same time. Heliocentric radius and latitude trajectories for both spacecraft as a function of Carrington rotation number are given in Figure 2. Details of the plasma observations during these time periods can be found in Rosenbauer *et al.* (1977) and Marsch *et al.* (1982*a*, *b*).

The solar wind seen by *Helios A* is characteristic of the near-minimum epoch of the past solar cycle, with one small and two large streams recurring in each of the rotations. A well-defined dipole sector structure is present during this period, and few flare-related shocks

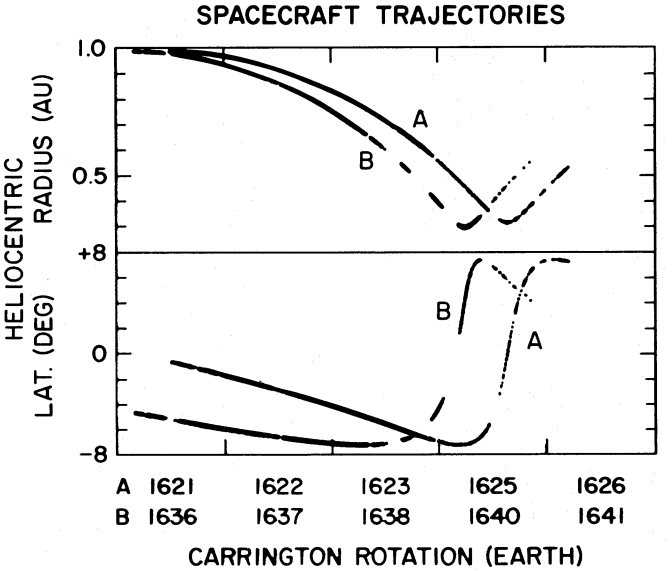

FIG. 2.—Orbital parameters for the primary mission of each spacecraft. Heliocentric radius (*top*) and latitude (*bottom*) are plotted as a function of Carrington rotation number (CR). Since the CR is figured relative to the Earth, the motion of the spacecraft results in a jump in the numbering sequence between the third and fourth rotations. Data gaps are indicated by breaks in lines.

or other major transients occurred (Richter and Hsieh, private communication 1981). *Helios B* observed the solar wind a full year later, but recurrent streams still dominated the large-scale variations within a dipole sector structure (Behannon, Neubauer, and Barnstorff 1981). Thus both spacecraft viewed essentially the same kind of solar wind.

Due to the high computational expense of the full 3D decomposition, only one spectrum in 10 is analyzed. That is, while each datum of our set represents one 40 s sample, these data are spaced 400 s apart. This latter temporal resolution results in little degradation of accuracy on the large scale and has even proven suitable for Alfvén wave studies (Marsch *et al.* 1981). Further, all the plasma data used in this analysis come from the I1a instrument only, as the amount of 3D data from I3 (the high-flux instrument used near perihelion) currently available is too limited to be of any use. The lack of the I3 data introduces a selection effect in the data for $r < 0.6$ AU, in that periods of cold, dense, slow speed flow are underrepresented. In light of the two-state nature of the flow near perihelion as reflected in all the other large-scale parameters (Rosenbauer *et al.* 1977), the intrinsic angular momentum content of the slow flows may systematically differ somewhat from that of the high-speed material. Therefore, we present the available 3D perihelion data with some caution.

b) Presentation of Raw Data

Figure 3 presents a scatter plot of all available 3D data for the two spacecraft. The total specific angular momentum flux (1) in units of 10^{30} dyn-cm sr^{-1} is plotted versus heliocentric radius in AU. There are three major aspects of this plot, to be discussed in turn.

i) *Scatter in the Observations*

There appear to be two distinct components in the observed scatter. One can be seen as a relatively dark horizontal band coincident with the apparent mean in both data sets. This component has a peak-to-peak magnitude of $\sim 6.0 \times 10^{30}$ dyn-cm sr^{-1} that does not show much variation with radius or between the two

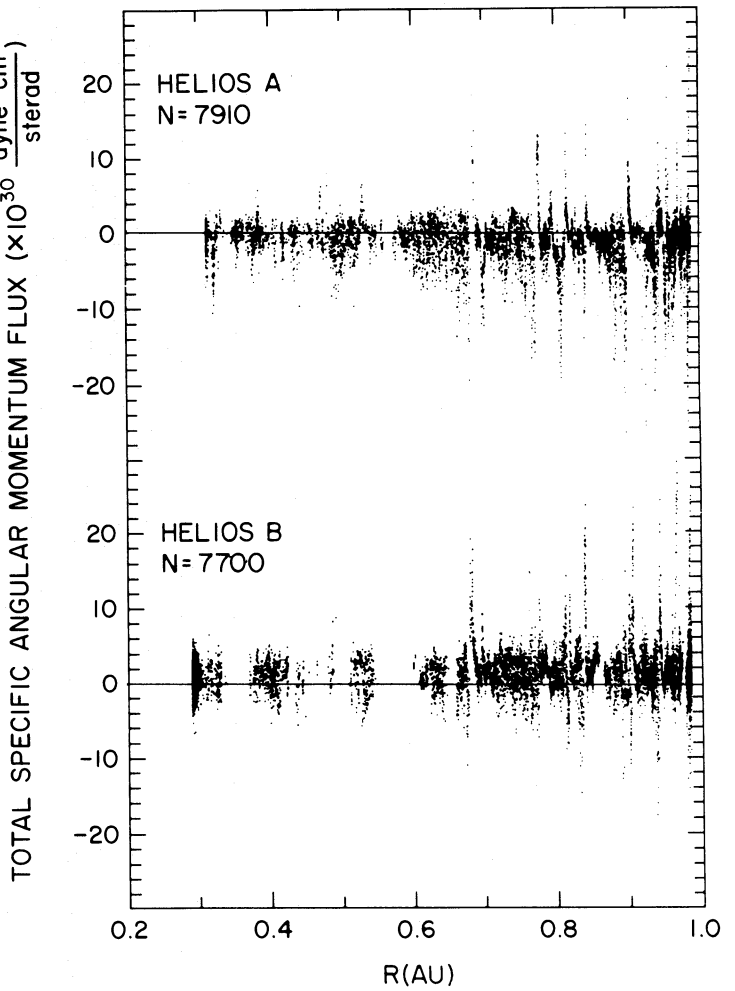

FIG. 3.—Scatter plot of all 3D data points from primary mission of each spacecraft. Figure shows total specific angular momentum flux (proton mechanical + alpha mechanical + magnetic stresses) versus heliocentric radius.

spacecraft. The magnitude of these fluctuations is consistent with saturated Alfvén waves, which are common in the interplanetary medium (see Villante 1980; Villante and Vellante 1982; Denskat, Neubauer, and Schwenn 1981). Farther from the Sun, the very large amplitude fluctuations are attributed to interplanetary dynamical processes. Near stream fronts, the interaction of high-speed streams with slower preceding flow along the interplanetary spiral gives rise to a systematic east-west deflection (Siscoe, Goldstein, and Lazarus 1969). While no angular momentum flux is generated globally in the process, these swings in flow direction show up as huge local fluctuations in proton angular momentum flux. More importantly, the magnitude of the fluctuations is sufficient to make the extraction of a reliable average a formidable task.

ii) *Radial Variation of the Scatter and Breakdown by Component*

In principle, the angular momentum flux is best measured near the Sun since simple conservation arguments dictate the average nonradial flow angle must increase at small r. What the plot above suggests is that the fluctuations about the average also decrease near the Sun. The reduction in noise level is dramatically displayed in Figure 4, which shows, side by side, *Helios A* data collected during two rotations. On the left is CR 1625 (Fig. 4*a*), during which *Helios A* achieved its first perihelion (cf. Fig. 2 for the corresponding spacecraft heliographic coordinates). The top panel presents the proton bulk velocity, with gaps in the 3D coverage filled in by 1D data. The other four panels depict specific angular momentum fluxes for the three components (proton mechanical, alpha mechanical, and magnetic field stresses) and the total, respectively, as functions of Carrington longitude. On the right (Fig. 4*b*) are data from CR 1622, when the spacecraft was near 1 AU. It is evident that the general level of fluctuations is much higher near 1 AU, with all three components showing systematic variations associated with stream fronts. Moreover, in both plots fluctuations in the protons appear to dominate the variations in the total. Hence eliminating the error in the proton angular momentum flux must be the primary concern of the analysis.

iii) *Offset between the Spacecraft*

Returning to Figure 3, there is an undeniable offset between eyeball estimates of the mean fluxes reported by the two spacecraft. On the face of it, the *Helios B* results are compatible with earlier findings from *Vela* and *Mariner*, while the *Helios A* findings lean toward the much-maligned negative values gleaned from *IMP* and *Pioneer*. It is hard to believe this can be a real effect.

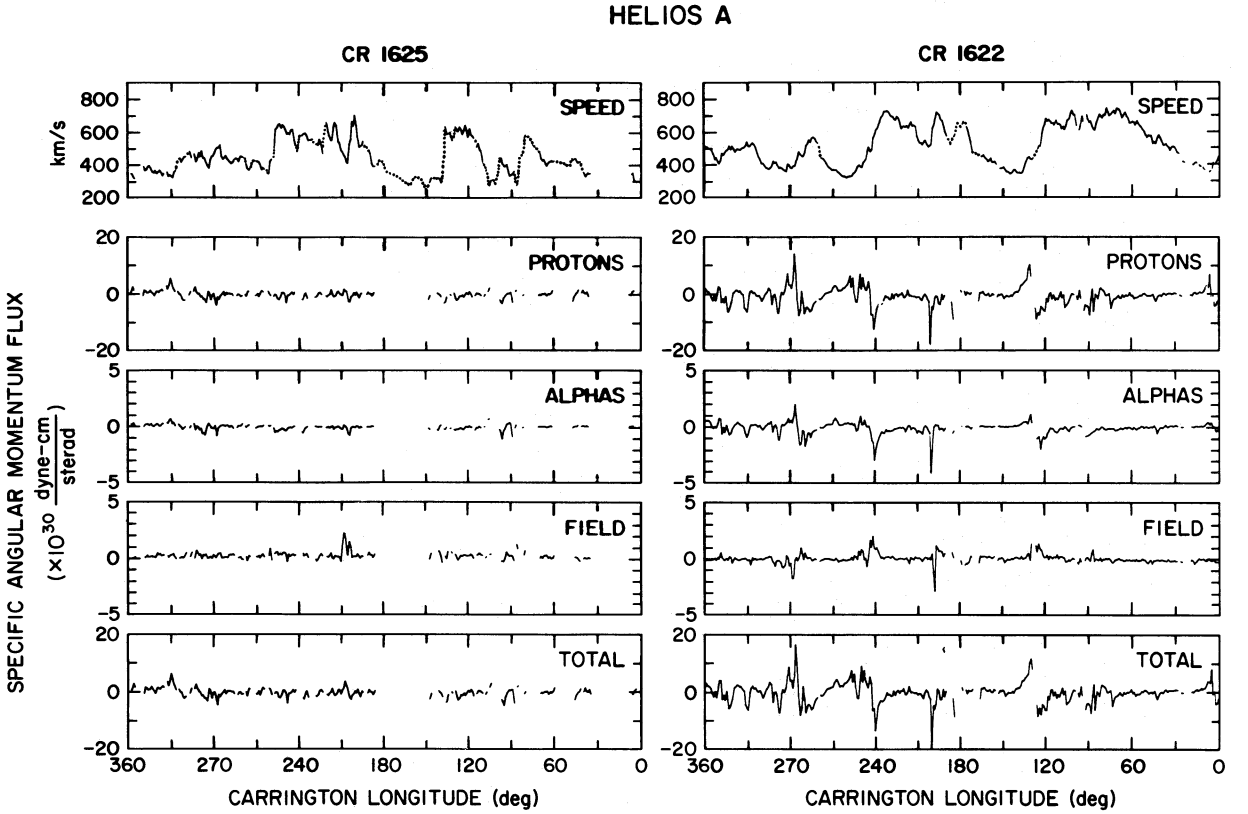

FIG. 4.—Breakdown of flux components for a rotation near the Sun (*left*) and far from the Sun (*right*). The panels show proton speed, F_p, F_α, F_B, and F, respectively. Note the change in scales between (F_p, F) and (F_α, F_B). An example of a transient deflection can be seen near longitude 200° of CR 1622, where a flare-related interplanetary shock was encountered.

We take this as evidence that something is wrong with the estimates of the angular momentum flux in the particles, that some systematic bias afflicts the analysis. Indeed, this suspicion is confirmed by a direct measurement of the angular offset between the two spacecraft during a period late in 1977 when the orbits of *Helios A* and *B* overlapped briefly. In a simultaneous sampling of the same plasma, the recorded proton flow angles were found to differ by some $2\overset{\circ}{.}2 \pm 0\overset{\circ}{.}2$. Unfortunately, this measurement provides no information as to the error for each spacecraft separately and in itself provides an incomplete basis for correction.

c) *Elimination of the Systematic Error and Quantitative Results*

The removal of the systematic error in the data follows from simple arguments and assumptions. This subsection opens with the demonstration that a common radial trend in total angular momentum flux exists in both *Helios A* and *B* data sets. Treating this trend as a misalignment of the coordinate axes, it is found that the radial trend is eliminated when the two data sets are rotated by a nearly equal and opposite amount in the r-ϕ plane. Such a correction is what would be naively expected from two identical spacecraft examining similar flows in the case that the systematic error is related to the sense of their opposed orientations in space. The validity of this argument is reinforced by the close agreement between the two spacecraft in average total azimuthal momentum flux, distribution of the flux among the species, flow angles, and other indicative parameters that emerges when the data are corrected in this way. More convincingly, it is in excellent agreement with the independent direct measurement of the net angular offset between the two spacecraft data sets mentioned above.

i) *Radial Trends in the Fluxes and Their Significance*

Figure 5 shows the specific angular momentum flux for all three components of both data sets (*Helios A*, open bars; *Helios B*, shaded bars) as a function of radius. The data have been averaged in radial bins chosen so that roughly the same standard error in the mean applies to each bin. The magnetic data (broken bars near center) can be dispensed with by noting only that the two data sets are in good agreement and that no radial trend is discerned. It is to be recalled that absolute orientation problems should have little effect here and therefore the magnetic flux determination should be the most reliable. The protons show distinct trends, which appear to be roughly linear with radius and oppositely directed. The alphas exhibit similar, though much weaker, radial variation.

The proton flux F_p in Figure 5 greatly exceeds the other two components in magnitude at all observed radii and is the source of the trend found in the total flux. But as detailed above, the proton flux is also the quantity most sensitive to alignment errors. In addition, it ought to be recognized that (1) large changes in the magnitude of the total angular momentum flux in this

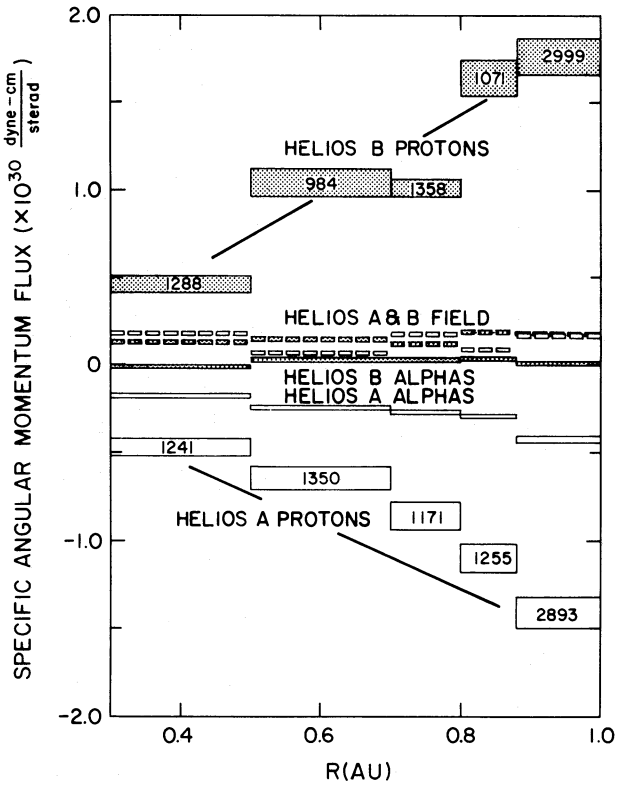

FIG. 5.—Radial variation of the component fluxes for each spacecraft. *Helios A* data are represented by open bars, *B* by shaded bars. The width of the bars indicates the radial span of the averaging bin, the height the standard error in the mean. The numbers within the proton bars specify the number of data points in the average. The magnetic data are presented as dashed or broken bars to differentiate them from the alphas.

radial range are at odds with theoretical expectations, unless there were a significant and highly variable latitudinal transport of angular momentum; (2) the parameter least sensitive to pointing errors—the magnetic component—shows no signs of any significant radial trends; and (3) were the raw proton fluxes real, inordinately large and suspiciously asymmetric, temporal and/or spatial variations in solar wind angular momentum transport would be implied. Figure 6, which depicts quantities not subject to the instrumental reservations voiced above, reveals no such variations but instead confirms that much the same sort of solar wind was encountered by the two probes. Hence there exist legitimate grounds for supposing that the radial trends in the particle data are largely spurious.

ii) *Elimination of the Trend*

Once it is accepted that the radial trends in the particle data are an empirical artifact, two logical methods to remove the bias can be imagined. The simpler method is based upon the *a priori* assumption of equal and opposite instrumental bias mentioned at the end of § IIIc. In that case, the mean particle

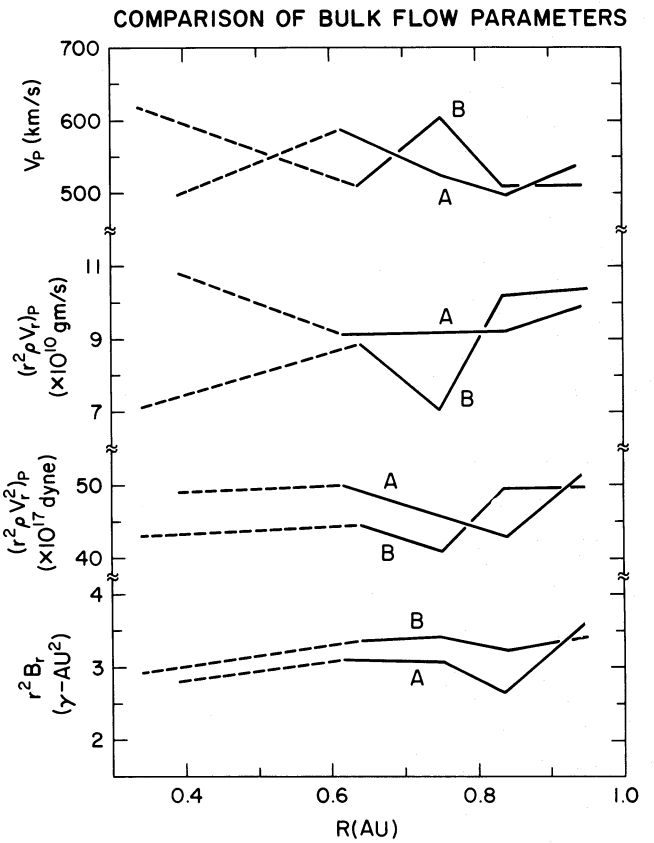

FIG. 6.—Comparison of bulk flow parameters for the two data sets. *From top*, proton speed, proton mass flux, proton mechanical radial momentum flux, and normalized radial magnetic field are shown as a function of radius. Dashed portions of the curves inside ~0.6 AU in this figure and the next are intended as a reminder of the selection effects mentioned in the text (§ IV*a*). These parameters are unaffected by small inaccuracies in spacecraft coordinates and demonstrate that both probes encountered similar solar wind conditions.

fluxes observed by the two spacecraft over some radial span are related to the real fluxes as

$$F^A_{\rm obs} = F^A_{\rm real} + \epsilon\,, \qquad F^B_{\rm obs} = F^B_{\rm real} - \epsilon\,, \tag{7}$$

where ϵ is the common systematic error. In principle, this method would be accurate for identical spacecraft observing identical flows; in practice, it must be applied in some average sense to a limited number of data collected at different times. The most cogent reason for avoiding this method, however, stems from the lack of internal consistency tests: only one set of averages emerges and there is no way to cross-check the basic assumptions between the two data sets.

Instead, we develop an alternate analysis that offers the advantage of internal consistency checks and, most importantly, provides a telling, independent observational test. Taking a cue from the discussion of § III*a*, we see that to the degree to which the average radial particle trends can be regarded as linear, the systematic bias can be viewed as a constant-angle pointing error, regardless of its true source. Correction can then be effected by a straightforward iterative procedure. The coordinates for the plasma data from each spacecraft are rotated in the r-ϕ plane by an angle $\delta\phi$, the appropriate flux quantities formed point by point, and the binned radial averages ascertained. The process is repeated for a range of $\delta\phi$ for each spacecraft, the aim being to find that $\delta\phi$ for which the total flux shows no trend, i.e., is constant with radius.

Figure 7 shows the total flux as a function of radius for three different angles ($\delta\phi = 0°$, $\pm 1.^\circ 2$, and $\pm 2.^\circ 4$) for each spacecraft. Because of the selection effect mentioned above, the data inside 0.6 AU have been plotted with dashed lines to indicate a higher degree of uncertainty in the averages. The sense of these corrections is such that the *Helios A* coordinate system is rotated in the negative (anti-corotating) direction while *Helios B* is just the opposite. It is seen in Figure 7 that both curves level out at about $\delta\phi = \pm 1.^\circ 2$ *and* at roughly the same positive total flux level, somewhere near 0.2 in these units. It is to be stressed that the only thing necessitated by our correction scheme is that there must be some $\delta\phi$ at which each curve will more or less level out. The fact that they do so at the same $|\delta\phi|$ and at the same absolute flux level may be nothing more than a beguiling coincidence, but we would argue that these agreements are consistent with the hypothesis that the

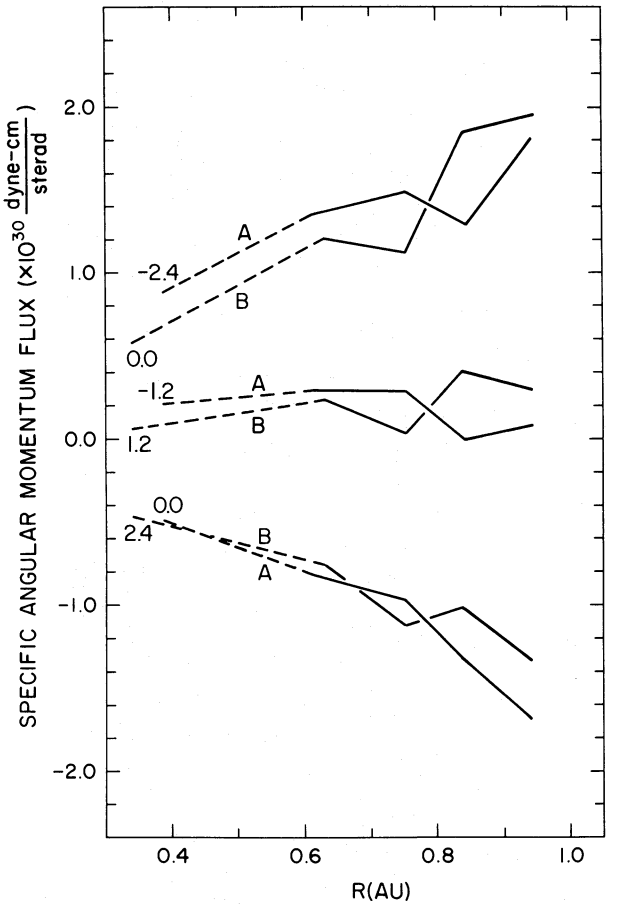

FIG. 7.—Corrected total flux as function of radius for both spacecraft. A simple rotational translation $\delta\phi$ is applied to the particle data before averaging in each case. The small numbers to the left of each curve indicate the value of $\delta\phi$. The figure shows that the radial trend is removed near $\delta\phi = \pm 1.^{\circ}2$, at which correction both spacecraft measure roughly the same total flux.

offset is due to a spin-related systematic error that is equal and opposite in the two spacecraft. Furthermore, the net angular offset implied by the correction, $|\delta\phi_A - \delta\phi_B| \approx 2.^{\circ}4$, compares very favorably with the direct measurement of $2.^{\circ}2 \pm 0.^{\circ}2$ mentioned previously.

We can offer additional corroborative evidence to support our method of removing the bias. First, the radial behavior of other flow parameters shows much more consistency with theoretical expectations and between the two spacecraft after correction. This point is illustrated in Figure 8, which shows average azimuthal velocities, $\langle u_\phi \rangle$, as a function of r for both spacecraft at $\delta\phi = \pm 1.^{\circ}2$ and for *Helios B* at $\delta\phi = 0$ (no correction). Proton data are shown as solid lines; alpha data, as dots. The uncorrected *Helios B* curves portray a rather strange radial evolution in $\langle u_\phi \rangle$ for both species: the protons are nearly constant at 11 km s^{-1} while the alphas swing over from negative to positive flow at 0.5 AU. The corrected data, however, display a much more palatable behavior: the protons have an average near zero and the alphas are strongly negative

TABLE 1

ESTIMATES OF AVERAGE SPECIFIC ANGULAR MOMENTUM FLUX FROM THE PRIMARY MISSION 3D DATA ($\delta\phi = \pm 1.^{\circ}2$)

Average Quantity ($\times 10^{30}$ dyn-cm sr^{-1})	*Helios A*	*Helios B*	Mean
F_p (protons)	0.15	0.19	0.17
F_α (alphas)	−0.13	−0.12	−0.13
F_B (field)	0.14	0.16	0.15
F (total)	0.16	0.23	0.20
$F_M \equiv \langle F_p + F_\alpha \rangle$ (particles)	0.02	0.07	0.05

over the entire span of radii, with clear traces of a $1/r$ falloff. As might be expected, the corresponding average flow angles are quite small, too, the 1 AU average for protons lying near $+0.^{\circ}2$ and that for the alphas near $-0.^{\circ}4$.

Second, under the applied correction, not only are the total flux magnitudes of the two spacecraft brought into agreement, but so also are the relative proportions of the three constituents. Figure 9 is a plot of the corrected radial averages for protons (*solid*), alphas (*dotted*), and field (*dashed*). The self-consistency of the data is readily apparent, with both spacecraft showing the same relative distributions of the three constituents. Table 1 summarizes the flux parameters averaged over

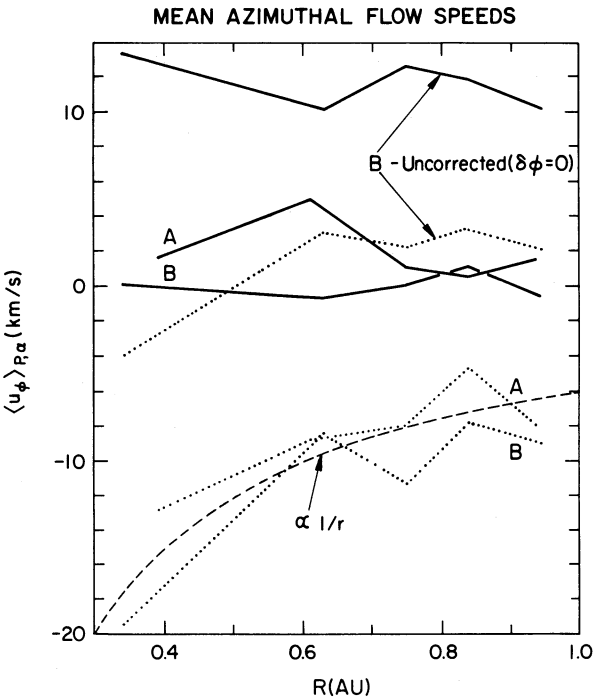

FIG. 8.—Radial variation in average azimuthal flow speed for protons (*solid*) and alphas (*dots*). Two of the curves depict uncorrected *Helios B* data. The other two pairs of curves show the corrected proton and alpha data for both spacecraft. Note how the average alpha flow speed is always more negative than the proton flow speed, in accordance with Fig. 1. For reference, the dashed curve through the corrected alphas traces a $1/r$ falloff.

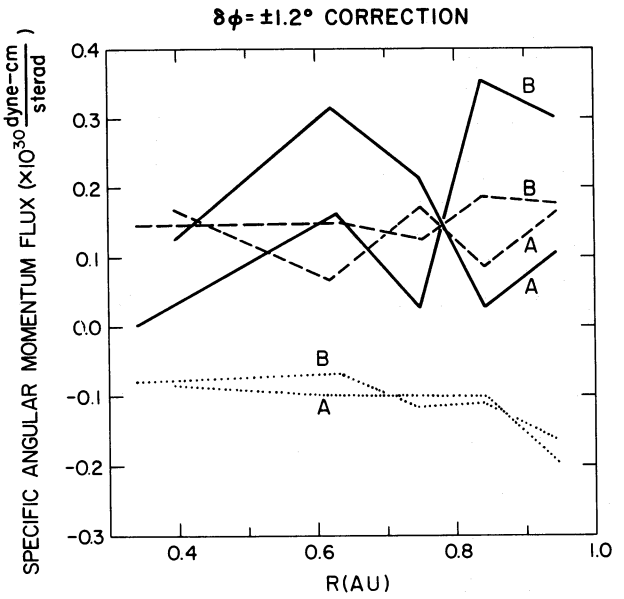

FIG. 9.—Corrected ($\delta\phi = \pm 1.^\circ 2$) radial averages for the three constituent angular momentum fluxes: protons (*solid*); alphas (*dotted*); and field (*dashed*).

the full 0.3–1.0 AU radial span for the two corrected data sets. Considering the large scatter in the raw data and all the other uncertainties involved, the corrected data show a rather remarkable agreement in all aspects. Furthermore, these estimates of the flux balance are together much closer to the original theoretical predictions than any heretofore reported. In particular, the mean ratio between particles and field (roughly 1:3) is very close to the Weber and Davis figure.

Because the $\delta\phi = \pm 1.^\circ 2$ correction is only approximate and the standard error bars shown in Figure 5 cannot be taken at face value (because much of the scatter is not random), we must resort to other means to gain some idea of the sensitivity of the results to

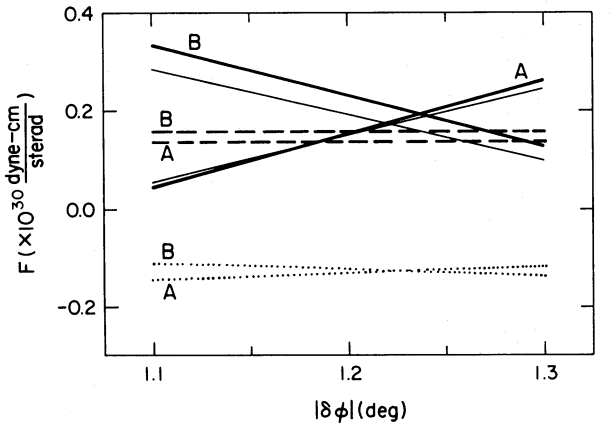

FIG. 10.—Dependence of the radially-averaged fluxes upon the correction angle, $\delta\phi$. The light solid line delineates the proton component, the dots the alphas, the dashes the field, and the heavy solid line the total. The A and B labels differentiate the curves for the two spacecraft.

the value of $\delta\phi$. Figure 10 shows a plot of the specific fluxes as a function of $\delta\phi$ for both spacecraft. Since it is hard to imagine that $|\delta\phi|$ can deviate more than a few tenths of a degree from the nominal $1.^\circ 2$ value, our basic results should not depend too critically on the precise value of $\delta\phi$. Inspection of Figures 9 and 10 suggests a realistic estimate of the error in any individual flux would perhaps lie in the neighborhood of 50%, with the greatest uncertainty in the protons.

V. ANALYSIS OF THE 1D DATA

As mentioned in § III*d*, the vast bulk of *Helios* plasma spectra are reduced by the more economical 1D method. This means that a great many more data may be examined, offering hopes of better statistical accuracy and enhanced confidence in the primary mission results. It also allows the study of some additional phenomena related to angular momentum transfer and demonstrates how minor differences in analysis techniques can have a major impact on angular momentum flux estimates.

a) Description of 1D Data Set

The analysis to follow makes use of the nearly 2 million plasma spectra obtained by the two spacecraft through mid-1980. This extensive collection covers a wide variety of solar wind flow states over a good portion of a solar cycle. About 10% of the data are from the I3 instrument (see § III*b*), which operates only at times of high mass flux inside 0.6 AU. Hence the full 1D data set is not afflicted with the selection effects that sully the near-Sun 3D results. On the other hand, the I3 data have to be calibrated separately against the I1a measurements, since the instrumental bias might not be identical. By comparing measured flow angles from periods when the two instruments were used alternately, it can be established that the I3 estimates are systematically shifted relative to the I1a values in such a way as to reduce the correction angle $\delta\phi$ by $0.^\circ 5$ in the case of *Helios A* and by $0.^\circ 6$ for *Helios B*. This additional correction must be applied before the I3 data are averaged in with the I1a observations.

While the usual magnetic data are available for the entire interval, the 1D analysis unfortunately provides no alpha flow angles and therefore no alpha angular momentum flux measurements. While it is possible to synthesize alpha flow angle data from the observed $\boldsymbol{u}_p$, $\boldsymbol{B}$, $|\boldsymbol{u}_\alpha|$, n_α and the assumption that $(\boldsymbol{u}_\alpha - \boldsymbol{u}_p) \times \boldsymbol{B} = 0$, in practice the 1D alpha separation proves unsuitable for such high precision work. Hence no estimate of the alpha angular momentum flux proceeds from the 1D analysis, nor can it provide an estimate of the total angular momentum loss rate, F.

b) 1D Results

The availability of so many proton data makes it feasible to segregate the measurements according to flow state. Figure 11 shows four histograms of F_p versus radius of each spacecraft, the topmost histogram referring to low-speed wind only, the next lower to

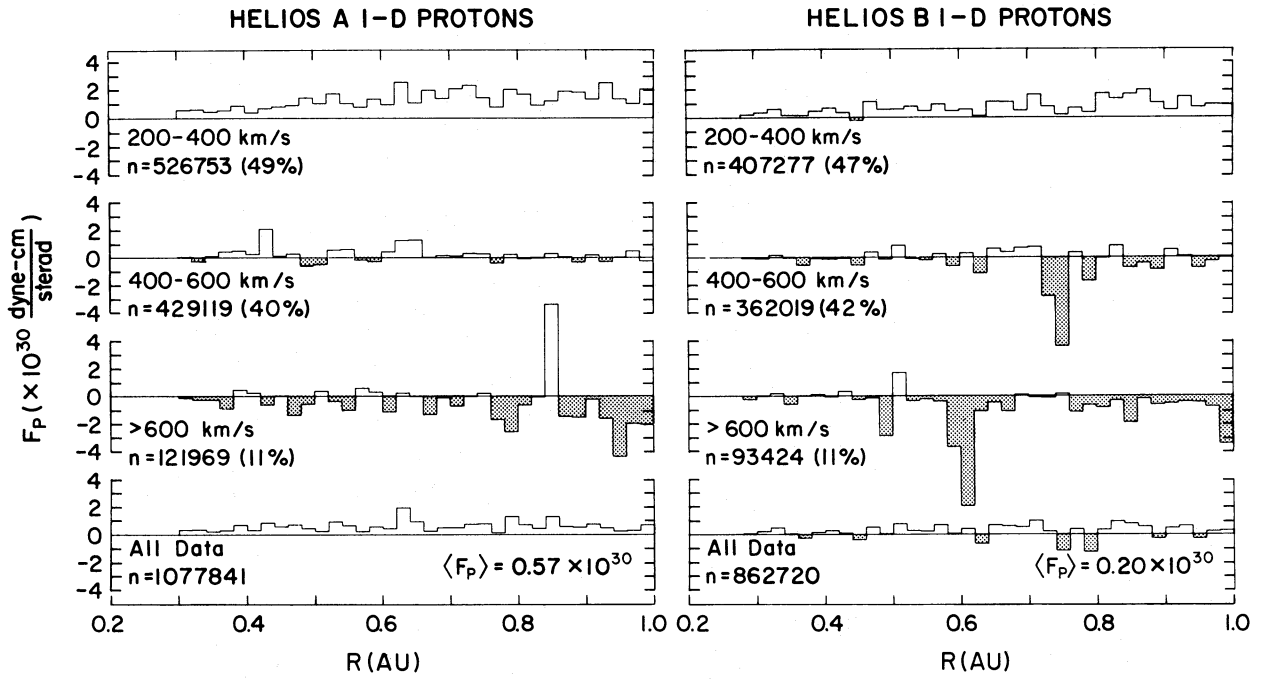

FIG. 11.—Histograms of proton angular momentum flux versus radius for spectra reduced by the 1D method. In the top three histograms, the data averaged in 0.02 AU bins are segregated according to flow speed, while the bottom one shows the composite. The numerals n refer to the total number of data points in each histogram, and the percentages in the parentheses list the fraction of all measures falling within that speed regime. The mean over all radii for the summed histograms is given at bottom as $\langle F_p \rangle$.

medium speed, the next to high speed, and the bottom one to the composite. The histograms reveal a number of interesting features. First, despite the large number of data points, the residual scatter in the histograms (as measured against the 3D estimate, $\langle F_p \rangle \approx 0.2 \times 10^{30}$ dyn-cm sr^{-1}) remains high, reflecting the inherent delicacy of the observation. Second, there is an obvious progression from slow to fast flow regimes, in that the former carries decidedly positive flux, the latter predominantly negative. Third, there is some evidence for the transfer of angular momentum from high-speed wind to low-speed wind with increasing heliocentric distance. This is most likely an artifact of the well-known east-west deflection at stream interaction fronts, whereby slow wind undergoes acceleration in the direction of corotation and fast solar wind is deflected in the opposite sense. Fourth, the composite histograms (bottom) suggest a slight positive net radial trend. This could be explained by a gradual transfer of momentum between alphas and protons arising from the requirement that the $(\boldsymbol{u}_\alpha - \boldsymbol{u}_p)$ vector lie along $\boldsymbol{B}$ and would be consistent with the negative trend in the alphas manifest in Figure 9. Finally, the *Helios A* estimates indicate a much more positive average flux, $\langle F_p \rangle = 0.57 \times 10^{30}$ dyn-cm sr^{-1}, than *Helios B*, $\langle F_p \rangle = 0.2 \times 10^{30}$. Also, the *Helios A* mean is at odds with the 3D determination reported above, though the *Helios B* value is very close to the latter.

The reality of the speed dependence in the mean proton flux appears to be pretty well established. It is present, to a lesser statistical reliability, in the 3D primary mission data, too. Table 2 summarizes a comparison of 1D and 3D mean flux estimates, broken down by component and speed regime. Values for each of the spacecraft as well as their net averages are given in units of 10^{30} dyn-cm sr^{-1}. The figures in the parentheses in the proton section refer to the fraction of the total data sample falling within each of the slow, mid, and fast flow classifications. While the absolute numbers differ somewhat among the various columns of the table, the basic speed-dependence effect for the protons is evident. The 3D data suggest a similar dependence for the alphas, but neither data set evinces such behavior on the part of the field. It might further be remarked that the ϵ-correction technique mentioned in conjunction with equations (7) yields averages very near the means listed in Table 2. Hence there is no reason to suppose the speed-dependence effect or other properties that may be inferred from the table are spurious artifacts of the constant-angle correction applied above. (See § VII for further discussion of the speed-dependence effect.)

It can be argued that the discrepancies in magnitude between the 1D *Helios A* and *B* fluxes and between the 1D and 3D means are more indicative of the inherent uncertainties in the proton determination than of any real variation. The disparities cannot be attributed to the inclusion of the I3 data in the 1D epoch, as elimination of these data does not materially alter the histograms or the averages. Furthermore, the I3 measurements

TABLE 2

1D AND 3D SPECIFIC ANGULAR MOMENTUM FLUXES[a] BY COMPONENT AND FLOW REGIME

	1D: ALL DATA THROUGH MID-1980 I1a + I3			3D: PRIMARY MISSION I1a only		
COMPONENT	*A*	*B*	Mean	*A*	*B*	Mean
Protons:						
Slow	1.22 (49%)	0.80 (47%)	1.01 (48%)	1.40 (22%)	2.51 (15%)	1.96 (19%)
Mid	0.13 (40%)	−0.29 (42%)	−0.08 (41%)	−0.01 (41%)	0.05 (41%)	0.02 (41%)
Fast	−0.72 (11%)	−0.49 (11%)	−0.70 (11%)	−0.43 (37%)	−0.48 (44%)	−0.46 (40%)
Sum	0.57	0.20	0.39	0.15	0.19	0.17
Alphas:						
Slow	...	...	...	0.11	0.15	0.13
Mid	...	...	...	−0.13	−0.13	−0.13
Fast	...	...	...	−0.28	−0.21	−0.25
Sum	...	...	...	−0.13	−0.12	−0.13
Field:						
Slow	0.16	0.21	0.18	0.09	0.19	0.14
Mid	0.20	0.24	0.22	0.15	0.17	0.16
Fast	0.17	0.13	0.16	0.15	0.14	0.15
Sum	0.18	0.21	0.19	0.14	0.16	0.15
Total:						
Slow	...	...	...	1.60	2.68	2.14
Mid	...	...	...	0.02	0.09	0.05
Fast	...	...	...	−0.56	−0.55	−0.56
Sum	...	...	...	0.16	0.23	0.20

[a] 10^{30} dyn-cm sr^{-1}.

are confined to the region inside 0.6 AU whereas the *Helios A–B* disparities in Figure 11 persist over the entire radial range. It is tempting to ascribe the difference between the 1D and 3D means to temporal effects, as high-flux slow-speed flows were encountered more than twice as often during the 1D epoch. On the other hand, the discrepancy between the individual 1D means for the two spacecraft, which report nearly identical sampling statistics, is at least as large as the 1D, 3D discrepancy, casting doubts on the temporal change explanation. In addition, the magnetic field averages show little hint of any systematic variation, which would be hard to reconcile with a real change in the proton flux of the magnitude implied by Table 2. Finally, even within a subset of the data, differences of 0.1–0.2 × 10^{30} dyn-cm sr^{-1} in the average proton fluxes as recorded by 1D and 3D analyses are not uncommon. Figure 12, for example, compares 3D (*solid*) and 1D (*dashed*) decompositions of the same raw spectra from a portion of the primary mission. The 1D values for both spacecraft show a net positive shift relative to the 3D result, the offset growing with radius. For *Helios A* the difference between the 1D and 3D $\langle F_p \rangle$ averaged over radius is +0.246 dyn-cm sr^{-1}, and for *Helios B* the figure is +0.172. These shifts, corresponding to an azimuthal velocity offset of the order of 1 km s^{-1}, could be expected to vary somewhat with the data sample. The precise reasons for these differences cannot be categorically identified, but at least two important contributing factors merit comment. The first point can be illustrated in terms of Figure 13, a schematic of a proton distribution function in the r-ϕ plane. In the 3D decomposition of such a spectrum the important plasma quantities like $|u|$, ϕ, n, etc., are determined from moments of a 3D piecewise parabolic interpolation of the observed spectra, with no *a priori* assumptions as to the shape of the distribution function. By contrast, the 1D method computes the flow parameters from a

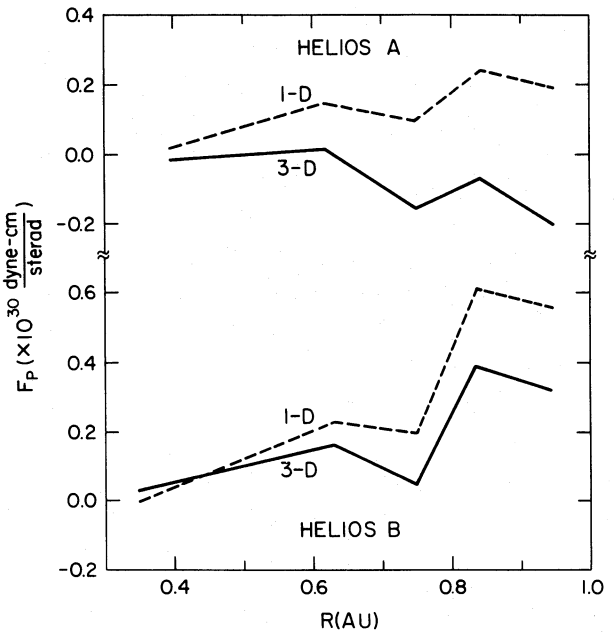

FIG. 12.—Differences in F_p between the 1D and 3D reduction methods for a subset of the primary mission data.

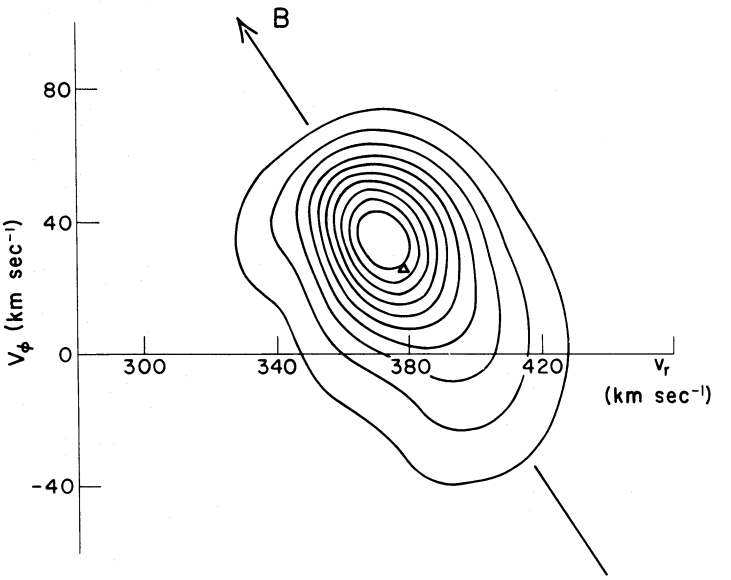

FIG. 13.—Schematic of a plasma distribution function in the r-ϕ plane. The diagonal line shows the field direction, and the small triangle marks the mean velocity (u_r, u_ϕ) of the skewed distribution. (Adapted from Hundhausen *et al.* 1967.)

Gaussian fit to the cores of the reduced distributions. When the plasma distribution function has a pronounced conductive tail (skew), the bulk velocity computed from the two methods must obviously differ slightly. Figure 13 depicts a typical near-Earth situation, where the diagonal line represents the average orientation of the interplanetary magnetic field in the r-ϕ plane. It is seen that the shift between the core centroid and the bulk velocity from a real moments' analysis amounts to a few km s^{-1} in the azimuthal direction. The effect is thus of the proper sign and magnitude to account for the 1D versus 3D offset of Figure 12, and has the proper radial behavior, too. But a second complication enters the picture, in that when the distribution function is very broad (high temperatures) or the azimuthal flow angle very large, a portion of the distribution slips out of the field of view of the instrument. (The instrumental field of view has an angular width of 33°.7 within a total range of −54°.5 to +32°.7 for *Helios A* and −48°.8 to +45°.3 for *Helios B*. The energy channels run from 0.155 keV to 15.32 keV.) The 3D decomposition treats the problem by extrapolating one additional grid point in the requisite direction; all flux beyond this artificial point is neglected in the subsequent analysis. Thus, where a substantial portion of the distribution is involved, the 1D method provides a more realistic extrapolation, so long as most of the core is registered. Clearly, under the conditions of high temperature and/or very large flow angles, the 3D estimates of the angular momentum flux must be spuriously low. Such occurrences, while not common, may also contribute to the flux discrepancies noted above.

Whatever the origin of the discrepancies, it must be borne in mind that they are still relatively small (corresponding to no more than 1 or 2 km s^{-1} error in u_ϕ at 1 AU) and that the means listed in Table 2 nonetheless represent a significant departure from previous estimates.

VI. SUMMARY OF RESULTS

Our results indicate a very different picture of solar wind angular momentum transport than previously reported. In consideration of the probable errors, our findings are best summarized as follows:

1. The magnitude of the total angular momentum flux is most probably in the range of 0.2–0.3 × 10^{30} dyn-cm sr^{-1}, about a factor of 3 or 4 lower than inferred from earlier solar wind observations.
2. The most accurately known component of the angular momentum flux, the magnetic field stress, is well established at about 0.15–0.2 × 10^{30}. This number is within a factor of 2 of the value reported in Lazarus and Goldstein (1971).
3. The angular momentum flux in the protons appears to be comparable to or perhaps slightly greater than that in the field, but this remains the most poorly determined of the major components of F.
4. The angular momentum flux in the alphas is a substantial fraction (roughly half) of that in the protons and is of the opposite sign.
5. The angular momentum flux in the particles (protons and alphas lumped together) is appreciably less than that in the magnetic stresses.
6. The average azimuthal flow angle and velocity at 1 AU appear to be low, a few tenths of a degree and 1 or 2 km s^{-1}, respectively, for protons, and about twice that (and negative) for the alphas.
7. There is a distinct tendency (increasing with heliocentric radius) for low-speed solar wind to carry positive proton flux and for high-speed wind to carry negative proton flux.
8. While it is difficult to come up with any rigorous

error estimates for all these results, a figure of $\pm 50\%$ for any value does not seem unreasonable.

Because we have not positively identified the physical cause of the systematic bias in the data, we cannot regard our interpretation of the raw data as unique. We argue that the interpretation and subsequent correction we have postulated are the simplest and most reasonable of the alternatives, barring the trivial response that there is just something pathologically wrong with the spacecraft and/or data analysis. Our interpretation leads to no obvious contradictions, requires no special or exotic physical mechanisms, and leads to a high level of mutual consistency in the two data sets, even down to detailed behavior in many parameters. Hence, while the intrinsic nature of the measurement precludes achieving the degree of certitude associated with most solar wind plasma experiments, we view the above results as accurately portraying the essential features of solar wind angular momentum transport with reasonable confidence.

VII. IMPLICATIONS FOR ASTROPHYSICS

There are two key features of the Weber and Davis (1967) model that can be directly compared with the *Helios* observations. The first is that the total angular momentum flux that escapes the Sun can be expressed in terms of two simple parameters. From the azimuthal equation of motion and the induction equation, it can be shown that L, the angular momentum loss per unit mass in the equatorial plane, is given by

$$L = \Omega r_A^2 = r\left(u_\phi - \frac{B_r B_\phi}{4\pi\rho u_r}\right)\Bigg|_{r=r_A}, \qquad (8)$$

where Ω is the solar rotation rate, ρ and u_ϕ refer to the single-fluid mass density and azimuthal velocity of the model, and r_A is the Alfvén radius, defined as the point where

$$4\pi\rho u_r^2/B_r^2 = 1 .$$

It is important to recognize that the simple expression $L = \Omega r_A^2$ remains valid even if there exist substantial sources and sinks of momentum not accounted for in the theory, so long as they are confined to the region inside r_A or strictly affect the radial motion only. The second important prediction of the model is that while the total angular momentum loss can be calculated *as if* the solar wind corotates out to r_A, most (about three-quarters) of the flux that escapes into the interplanetary region should be carried by the field stresses. The average azimuthal velocity at 1 AU should then be very small, on the order of 1 km s^{-1}.

Our analysis of the *Helios* data shows that the total flux in the ecliptic plane is a factor of 3 or 4 smaller than predicted by the Weber and Davis theory. The reduction in the total flux can be readily accounted for by noting that the 1 AU field strength ($B_r = 5\gamma$) used in the Weber and Davis calculations is somewhat high (cf. Fig. 6) and that the Alfvén radius lying at 24.3 $R_\odot$ in their polytropic description is strongly model dependent. Since the specific angular momentum flux, $L(\rho u_r r^2)$, varies as r_A^2 via (8), we see that our observations imply a mean Alfvén radius in the range 12–14 $R_\odot$. Such a value for r_A is not at all unrealistic. Isothermal models, which presumably provide a lower limit on r_A, can push the Alfvén radius all the way down to 2.5 $R_\odot$ (e.g., Pneuman and Kopp 1971), while conductive models favor somewhat higher figures (10–60 $R_\odot$, e.g., in Durney and Pneuman 1975), depending upon local flow conditions. Even simple extrapolation of spacecraft data back to the Sun suggests an r_A in the 12 $R_\odot$ range. Table 3 lists typical bulk parameters from *Helios* within the broad, roughly uniform flow found at the center of two high-speed streams encountered at $\sim$0.3 AU in the primary mission. Assuming constant radial velocity u_p and $1/r^2$ behavior for proton density n_p and radial magnetic field B_r, we find that the Alfvén speed $V_A = (B_r^2/4\pi\rho)^{1/2}$ equals u_p at the indicated distances. A similar mapping of the intrinsically more variable low-speed flows yields estimates in the neighborhood of 10–40 $R_\odot$.

The geometry of the coronal expansion also influences the total angular momentum flux imparted to the wind. Priest and Pneuman (1974), using the single-fluid isothermal MHD model of Pneuman and Kopp (1971), found that the global (integrated over 4π) angular momentum loss in the more realistic case of an axisymmetric, equatorial dipole flow was an order of magnitude less than that of the equivalent monopolar expansion, such as presumed in the Weber and Davis model. What happens is that the portion of the lower corona shut off from the solar wind by closed field lines does not participate in the angular momentum loss at all, while the rapid expansion of the remaining open field regions results in a general lowering of the Alfvénic surface, particularly in the vicinity of the equatorial current sheet. It can be inferred from their presentation that the angular momentum flux near the equator is reduced by a factor of 5 from the monopolar equivalent.[3] While it must be cautioned that this model suffers from the usual theoretical difficulties in simultaneously matching flow conditions over the full Sun-Earth distance and while the assumed coronal structure is highly idealized, the qualitative theoretical

[3] These figures reflect a correction to the monopolar r_A quoted by Priest and Pneuman from 7.7 $R_\odot$ to 9.9 $R_\odot$; cf. Skumanich and Eddy (1981).

TABLE 3

TYPICAL FLOW PARAMETERS IN HIGH-SPEED MATERIAL NEAR PERIHELION OF *Helios* PRIMARY MISSIONS

Parameter	*Helios A*	*Helios B*
r(AU)	0.31	0.29
n_p(cm^{-3})	30	30
v_p(km s^{-1})	650	750
$B_r(\gamma)$	30	35
$r_A(R_\odot)$	12.6	11.5

assessment that geometric effects are likely to significantly depress the angular momentum loss below the Weber and Davis prediction is consistent with our observations, at least within the ecliptic plane. Comment on the global aspects of the problem is, of course, beyond the ken of the *Helios* investigation and must await whatever can be gleaned from the *Solar Polar Mission.*

The Priest and Pneuman (1975) study deals with latitudinal structure only, whereas the real solar wind is subject to longitudinal variations as well. There is reason to believe that the speed dependence of the angular momentum flux (cf. § V*b* and Fig. 11) is a manifestation of the dynamical interaction between quasi-steady corotating streams arising from the longitudinal structure of the corona. The main arguments in favor of this hypothesis are that the effect is found only in the particles and that it gains rapidly in prominence beyond about 0.5 AU, just where the stream activity picks up strongly (e.g., see the systematic deflections in the scatter plot of Fig. 3). Were the speed dependence an intrinsic effect (i.e., should low and high speed flows experience fundamentally different coupling with the coronal rotation, something beyond the scope of the Weber and Davis description), it would be natural to expect some relic of the difference to appear in the magnetic stresses. No such evidence is found (cf. Table 2). It might be added that the magnitude of the slow-fast shift in the proton flux near 0.3 AU would imply a systematic flow angle offset between slow and fast streams of only about 2°. A stream-interaction deflection of this small size in the region between the corona and 0.3 AU does not seem at all objectionable on dynamical grounds. In the absence of any compelling reason to interpret the speed-dependence effect as signaling some catastrophic failure of the Weber and Davis theory, then, dynamics appear the best explanation. (But see also the Appendix.)

Our second major observational result is that the distribution of angular momentum flux between particles and field appears to be consistent with the prediction of the theory, that most of the flux in interplanetary space should be in the field. As the transfer of momentum between particles and field occurs very low in the corona, it is to be expected that a twofold reduction in r_A, which is suggested by our estimate of the total flux, should have little impact upon the predicted distribution of flux. Therefore, we interpret this coarse agreement as support for the hypothesis that the magnetic field is the prime mechanism by which angular momentum is transported from the Sun and it is the magnetic field which exerts the major torque on the interplanetary plasma. It is noteworthy that the only models which succeeded in transferring a large amount of flux to the particles (e.g., Weber 1970; Weber and Davis 1970; Schubert and Coleman 1968) were the ones wherein all relevant variables were not self-consistently calculated, i.e., the effect was essentially computed as a correction upon a specified initial flow state. Since the zero-order angular momentum is already a very small quantity that is manifestly sensitive to the $u_r(r)$ profile near the Sun, it must be questioned whether anything short of a complete calculation is to be trusted. Significantly, the models that do include fully self-consistent treatment of all variables [most importantly, $u_r(r)$] uniformly show little increase in u_ϕ, despite their probable overestimate of viscous and conductive effects stemming from use of classical transport coefficients (e.g., see Leer and Holzer 1972). Hence, we see no need to continue pursuit of exotic mechanisms or superposition of numerous small effects with the object of enhancing the proportion of angular momentum flux carried by the particles. Rather, we view the basic Weber and Davis (1967) model as adequately describing the physical interaction coupling the rotation of a star with its associated wind, insofar as simple magnetic stresses are taken as the principal physical mechanism.

The one cautionary note that must be sounded, however, relates to the alpha-proton speed difference. Within a single-fluid description like the Weber and Davis model, differences in bulk speed between alphas and protons show up as an anisotropic pressure, even in the limit of zero species temperature (cf. Appendix). For speed differences of the magnitude seen in high-speed flows near 0.3 AU ($\sim$150 km s^{-1}), this pressure anisotropy becomes important, in the sense that neglect of the alphas produces a very distorted impression of the angular momentum flux in the particles. On the other hand, as evidenced by the good agreement between the observed and predicted distribution of flux, the anisotropy does not appear to transfer much momentum from field to particles in the aggregate: it merely acts to redistribute what is already there, to effect an exchange of momentum between protons and alphas. This is the sort of behavior one might anticipate if the alpha-proton speed difference originates in the super-Alfvénic region, where the pressure gradients are small. In the case of the Sun, it is pretty well established that the energy and/or momentum addition required to drive high-speed streams must occur above 2 $R_\odot$ and perhaps a good deal farther out (Leer, Holzer, and Flaa 1982). Presumably, this same heating is responsible for the alpha-proton speed differences, and should therefore have little influence on the net angular momentum transport. For the more general case of stellar winds, however, there may be situations where extended heating of the sort invoked for high-speed solar wind streams may take place quite low in the atmosphere, down where the Weber and Davis model postulates the bulk of the angular momentum transfer is effected. To describe the coupling in that instance, it may be necessary to develop a multifluid version of the model, for the anisotropy term may then become important. These considerations may have particular significance for radiatively driven winds, wherein the various ions are subject to large differential accelerations.

As the Sun is a slowly rotating star with relatively weak fields, a precise determination of the angular momentum flux is of limited value in itself. The effect

on the present-day Sun is negligible, and any small number for the angular momentum loss fits nicely with the simplistic *e*-folding time estimates for solar spin-down (e.g., Brandt 1966). The real impact of our work would appear to be felt in stellar rotation studies where the Weber and Davis theory may now be applied with enhanced confidence. For rapidly spinning objects, stellar winds may significantly brake the rotation in times short compared with the life of the star, with interesting consequences for the internal structure and subsequent evolution. Investigations of this sort, which require application of the Weber and Davis model over a much broader parameter range than appears in the original work, would probably benefit from suitable modifications to account for helium content, coronal acceleration mechanisms, and 3D effects, (e.g., see Skumanich and Eddy 1981 for a discussion of how geometric effects affect the stellar rotation–inverse square root age relation).

The authors wish to thank A. J. Hundhausen for a careful reading of the manuscript and T. E. Holzer, A. K. Richter, and W. I. Axford for useful discussions and comments. Acknowledgment is also due to K. Koppel, who patiently typed numerous drafts of this work, and to the referee for his useful comments. V. P. would like to express his gratitude to all the members of the MPAe staff, who made his stay at the Institute both fruitful and memorable.

The *Helios* plasma experiment and its data evaluation are supported by the German Bundesministerium für Forschung und Technologie under grants WRS 10/7 and WRS 0108.

APPENDIX

SINGLE-FLUID PRESSURE ANISOTROPY IN THE PRESENCE OF AN ALPHA-PROTON SPEED DIFFERENTIAL

The derivation of the MHD equations begins with the taking of moments of the kinetic equation for each species (e.g., Boyd and Sanderson 1969). The first moment, which ultimately gives rise to the usual momentum equation, contains the dyadic term

$$\nabla \cdot (mn\langle \boldsymbol{v} v_i \rangle) , \tag{A1}$$

where m is the species mass, n the species density, $\boldsymbol{v}$ the particle velocity, v_i its ith component, and the angle brackets denote the average over phase space. The center-of-mass velocity, $\boldsymbol{U}$, is defined as

$$\boldsymbol{U} = \frac{\sum mn\boldsymbol{u}}{\sum mn} ,$$

where the sums are over the species and $\boldsymbol{u}$ is the local mean velocity of each species, defined by $\boldsymbol{u} = \langle \boldsymbol{v} \rangle$.

To evaluate (A1), we need to form the average $\langle v_j v_i \rangle$. In the single-fluid description, $\boldsymbol{w}$, the random velocity of a particle, is taken relative to the center-of-mass velocity, $\boldsymbol{U}$. Thus,

$$\boldsymbol{w} \equiv \boldsymbol{v} - \boldsymbol{U} . \tag{A2}$$

Then, for each species,

$$\langle v_j v_i \rangle = \langle (w_j + U_j)(w_i + U_i) \rangle = \frac{p_{ji}}{mn} + w_j U_i + w_i U_j + U_j U_i , \tag{A3}$$

where p_{ji} is the partial pressure, $p_{ji} = p_{ij} \equiv mn\langle w_j w_i \rangle$. When (A3) is inserted into (A1) and summed over species, we obtain the familiar result

$$\frac{\partial}{\partial r_j} [P_{ji} + \rho U_j U_i] = \nabla \cdot [\mathbf{P} + \rho \boldsymbol{U}\boldsymbol{U}] . \tag{A4}$$

Here we have made use of the definition of $\boldsymbol{U}$ and have introduced $P_{ji} = \sum p_{ji}$ and $\rho = \sum mn$.

Suppose that instead of (A2) we define the random velocity about the species average, i.e.,

$$\boldsymbol{c} \equiv \boldsymbol{v} - \boldsymbol{u} . \tag{A5}$$

Then

$$\langle v_j v_i \rangle = \langle (c_j + u_j)(c_i + u_i) \rangle = \frac{\pi_{ji}}{mn} + u_j u_i , \tag{A6}$$

in analogy to (A3). Here $\pi_{ji} \equiv mn\langle c_j c_i \rangle$ is the species partial pressure, and $\langle c \rangle = 0$. The divergence expression, when summed over species, is just

$$\frac{\partial}{\partial r_j}[\sum \pi_{ji} + \sum mnu_j u_i] . \tag{A7}$$

We now relate (A7) to the center-of-mass expression (A4) by making the substitution $\boldsymbol{u} = \boldsymbol{U} + \delta\boldsymbol{u}$, where $\delta\boldsymbol{u}$ is the difference vector between each species mean velocity and $\boldsymbol{U}$. Plugging in, we obtain

$$\frac{\partial}{\partial r_j}[\sum \pi_{ji} + \rho U_j U_i + \sum mn(U_j \delta u_i + \delta u_j U_i + \delta u_j \delta u_i)] .$$

The terms linear in δu, which simply represent weighted sums of the species deviation from the center-of-mass speed, can readily be shown to vanish individually. Thus the final expression for the divergence term is

$$\frac{\partial}{\partial r_j}[\sum \pi_{ji} + \rho U_j U_i + \sum mn\delta u_j \delta u_i] . \tag{A8}$$

Comparing with (A4), we see that the pressure tensor can be written as

$$P_{ji} = \sum \pi_{ji} + \sum mn\delta u_j \delta u_i \equiv \sum \pi_{ji} + d_{ji} . \tag{A9}$$

This expression illustrates why it is inadmissible to directly add partial pressures; the correction **d** must be made to account for the differences in the definition of the random velocities. This differential stress is implicitly included in the three-fluid conservation expression (1).

For a proton-electron gas, the usual single-fluid description of the solar wind, we expect **d** to be quite small: the weak magnetic fields in interplanetary space imply small currents and hence little velocity difference between protons and electrons. This, coupled with the huge relative mass of the protons, ensures that the net anisotropy of the fluid is dominated by the species partial pressure term, $\sum \pi_{ji}$. For typical solar wind conditions, this means the anisotropy in P_{ji} will look like a diluted version of the proton anisotropy. When alphas are brought into the picture, however, the ionic $\delta\boldsymbol{u}$'s can be of the order of the thermal speed, and a large contribution to the net anisotropy now comes from **d**. Furthermore, (A9) shows that even in the limit of zero species temperature, the fluid as a whole feels a stress due to the alpha-proton speed difference.

The behavior of the net pressure tensor when **d** is important can differ sharply from the assumptions in previous studies of thermal anisotropy effects. To illustrate this, we express **d** in an orthogonal coordinate system where the $\hat{e}_\parallel$ axis lies along the magnetic field. Since observation (Asbridge *et al.* 1976; Marsch *et al.* 1981, 1982*a*) indicates the alpha-proton speed difference lies in this direction, to a very good approximation $\mathbf{d} = \sum mn\delta u \delta u \hat{e}_\parallel \hat{e}_\parallel$. Expanding the sum, we find

$$\mathbf{d} = \{\rho_p[(\boldsymbol{u}_p + \boldsymbol{U}) \cdot \hat{e}_\parallel]^2 + \rho_\alpha[(\boldsymbol{u}_\alpha - \boldsymbol{U}) \cdot \hat{e}_\parallel]^2 + \rho_e[(\boldsymbol{u}_e - \boldsymbol{U}) \cdot \hat{e}_\parallel]^2\}\hat{e}_\parallel \hat{e}_\parallel \approx \frac{\rho_p \rho_\alpha}{\rho}[(\boldsymbol{u}_\alpha - \boldsymbol{u}_p) \cdot \hat{e}_\parallel]^2 \hat{e}_\parallel \hat{e}_\parallel ,$$

where the subscripts denote protons, alphas, and electrons. In spherical coordinates,

$$\mathbf{d} = \frac{\rho_p \rho_\alpha}{\rho}(\Delta u)^2[\cos^2 \psi \hat{e}_r \hat{e}_r - \cos \psi \sin \psi(\hat{e}_r \hat{e}_\phi + \hat{e}_\phi \hat{e}_r)] , \tag{A10}$$

where ψ is the angle between the radius vector and the field (and in the direction of corotation) and Δu is the magnitude of the alpha-proton speed difference vector. The torque on the fluid due to the anisotropy is given by

$$(\nabla \cdot \mathbf{P})_{r\phi} = \frac{1}{r^2}\frac{\partial}{\partial r}(r^2 P_{r\phi}) .$$

We therefore compare the radial variation of $d_{r\phi}$ in (A10) with that of the assumed $P_{r\phi}$ in Weber (1970) and Weber and Davis (1970). They had

$$P_{r\phi} = -(\sin^2 \psi P_\parallel) \cos \psi \sin \psi . \tag{A11}$$

The salient difference between (A10) and (A11) is the coefficient of the $\cos \psi \sin \psi$ geometric term. In interplanetary space near the Sun, $\cos \psi \sin \psi \sim r$, $\sin^2 \psi \sim r^2$, and $P_\parallel \sim r^{-10/3}$ (assuming constant speed, adiabatic flow). Thus, in the Weber and Davis prescription (A11), $r^2 P_{r\phi} \sim r^{5/3}$ and the torque is strongly positive, i.e., the field transfers momentum to the particles. For the speed differential tensor (A10) in fast streams beyond 0.3 AU, the density term drops off like r^{-2} while Δu roughly follows the Alfvén speed and consequently declines like r^{-1}. Accordingly, $r^2 d_{r\phi} \sim r^{-1}$, and the divergence is negative and appreciably smaller in magnitude than the Weber and Davis expression. Therefore, while a significant fraction of the angular momentum flux may lie in the anisotropy term,

in this case the anisotropic stress relaxes primarily by equilibrating the alpha and proton velocities without decelerating the fluid as a whole very much. The near-Sun variation of $d_{r\phi}$, on the other hand, may be of quite different nature. Here Δu must be increasing, perhaps rapidly, over some interval associated with whatever initiates the alpha-proton speed differential. In that case, the fluid would indeed be spun up, perhaps vigorously, particularly if the action takes place much inside r_A. This mechanism might be important for radiatively driven winds, too, provided thermalization effects do not equilibrate the ionic speeds too quickly.

Attempts at more categorical statements on this subject unfortunately stray into the realm of idle speculation. Too little is known about the nature of the alpha-proton speed difference in the all-important region of the corona, and, owing to the recognized sensitivity of even the single-fluid solutions to self-consistency deficiencies, anything short of a full three-fluid extension of the Weber and Davis model seems likely to produce specious results.

REFERENCES

Acuña, M. H., and Whang, Y. C. 1976, *Ap. J.*, **203**, 720.
Alfonso-Faus, A. 1968, *Planet. Space Sci.*, **16**, 1.
Asbridge, J. R., Bame, S. J., Feldman, W. C., and Montgomery, M. D. 1976, *J. Geophys. Res.*, **81**, 2719.
Behannon, K. W., Neubauer, F. M., and Barnstorff, H. 1981, *J. Geophys. Res.*, **86**, 3273.
Boyd, T. J. M., and Sanderson, J. J. 1969, *Plasma Dynamics* (New York: Barnes & Noble), chap. 3.
Brandt, J. C. 1966, *Ap. J.*, **144**, 1221.
———. 1967, *Ap. J.*, **147**, 201.
Brandt, J. C., and Heise, J. 1970, *Ap. J.*, **159**, 1057.
Brandt, J. C., Wolff, C., and Cassinelli, J. P. 1969, *Ap. J.*, **156**, 1117.
Denskat, K. U., Neubauer, F. M., and Schwenn, R. 1981, *Solar Wind Four* (MPAE-W-100-81-31, Lindau, FRG), p. 392.
Dicke, R. H. 1964, *Nature*, **202**, 432.
Durney, B. R., and Pneuman, G. W. 1975, *Solar Phys.*, **40**, 461.
Egidi, A., Pizella, G., and Signorini, C. 1969, *J. Geophys. Res.*, **74**, 2807.
Ferraro, V. C. A., and Bhatia, V. B. 1967, *Ap. J.*, **147**, 220.
Hardrop, J. 1971, *Astr. Ap.*, **14**, 210.
Hollweg, J. V. 1973, *J. Geophys. Res.*, **78**, 3643.
Hundhausen, A. J. 1972, *Coronal Expansion and Solar Wind* (New York: Springer), chap. III.15.
Hundhausen, A. J., Bame, S. J., Asbridge, J. R., and Sydoriak, S. J. 1970, *J. Geophys. Res.*, **75**, 4643.
Hundhausen, A. J., Bame, S. J., and Montgomery, M. D. 1970, *J. Geophys. Res.*, **75**, 4631.
Hundhausen, A. J., Bame, S. J., and Ness, N. F. 1967, *J. Geophys. Res.*, **72**, 5265.
Könemann, B., and Schröder, H. 1974, *Planet. Space Sci.*, **22**, 321.
Lazarus, A. J., and Goldstein, B. E. 1971, *Ap. J.*, **167**, 571.
Leer, E., and Holzer, T. E. 1972, *J. Geophys. Res.*, **77**, 4035.
Leer, E., Holzer, T. E., and Flaa, T. 1982, *Space Sci. Rev.*, **33**, 161.
Marsch, E., Mühlhäuser, K.-H., Rosenbauer, H., Schwenn, R., and Denskat, K. U. 1981, *J. Geophys. Res.*, **86**, 9199.
Marsch, E., Mühlhäuser, K.-H., Rosenbauer, H., Schwenn, R., and Neubauer, F. M. 1982*a*, *J. Geophys. Res.*, **87**, 35.
Marsch, E., Mühlhäuser, K.-H., Schwenn, R., Rosenbauer, H., Pilipp, W., and Neubauer, F. M. 1982*b*, *J. Geophys. Res.*, **87**, 52.
Mestel, L. 1968, *M.N.R.A.S.*, **138**, 359.
Modisette, J. L. 1967, *J. Geophys. Res.*, **72**, 1521.
Musmann, G., Neubauer, F. M., Maier, A., and Lammers, E. 1975, *Raumfahrtforschung*, **19**, 232.
Nerney, S. F., and Suess, S. T. 1975, *Ap. J.*, **200**, 503.
Neubauer, F. M., Beinroth, H. J., Barnstorf, H., and Dehmel, G. 1977, *J. Geophys.*, **42**, 599.
Neugebauer, M., Wu, C. S., and Huba, J. D. 1978, *J. Geophys. Res.*, **83**, 1027.
Parker, E. N. 1958, *Ap. J.*, **128**, 664.
Pizzo, V. J. 1982, *J. Geophys. Res.*, **87**, 4374.
Pneuman, G. W. 1966, *Ap. J.*, **145**, 800.
Pneuman, G. W., and Kopp, R. A. 1971, *Solar Phys.*, **18**, 258.
Priest, E. R., and Pneuman, G. W. 1974, *Solar Phys.*, **34**, 231.
Rosenbauer, H., Schwenn, R., Marsch, E., Meyer, B., Miggenrieder, H., Montgomery, M. D., Mühlhäuser, K.-H., Pilipp, W., Voges, W., and Zink, S. M. 1977, *J. Geophys.*, **42**, 561.
Schubert, G., and Coleman, P. J. 1968, *Ap. J.*, **153**, 943.
Schwenn, R., Rosenbauer, H., and Miggenrieder, H. 1975, *Raumfahrtforschung*, **5**, 226.
Siscoe, G. L., Goldstein, B., and Lazarus, A. J. 1969, *J. Geophys. Res.*, **74**, 1759.
Skumanich, A., and Eddy, J. 1981, in *Solar Phenomena in Stars and Stellar Systems* (Proc. NATO ASI, Bonas, France, 1980), ed. R. M. Bonnet and A. Dupree (Dordrecht: Reidel).
Solar Wind. 1972, ed. C. P. Sonett, P. J. Coleman, Jr., and J. M. Wilcox (NASA SP-308), p. 261.
Strong, I. B., Asbridge, J. R., Bame, S. J., and Hundhausen, A. J. 1967, in *Zodiacal Light and Interplanetary Medium*, ed. J. Weinberg (NASA SP-150).
Urch, I. H. 1969, *Solar Phys.*, **10**, 219.
Villante, U. 1980, *J. Geophys. Res.*, **85**, 6869.
Villante, U., and Vellante, M. 1982, *Solar Phys.*, **81**, 367.
Weber, E. J. 1969, *Solar Phys.*, **9**, 150.
———. 1970, *Solar Phys.*, **13**, 240.
Weber, E. J., and Davis, L., Jr. 1967, *Ap. J.*, **148**, 217.
———. 1970, *J. Geophys. Res.*, **75**, 2419.
Wolfe, J. H. 1972, in *Solar Wind*, ed. C. P. Sonett, P. J. Coleman, Jr., and J. M. Wilcox (NASA SP-308), p. 170.
Wolff, C. L., Brandt, J. C., and Southwick, R. G. 1971, *Ap. J.*, **165**, 181.

E. MARSCH, H. ROSENBAUER, and R. SCHWENN: Max-Planck-Institut für Aeronomie, Postfach 20, 3411 Katlenburg-Lindau 3, Federal Republic of Germany

K.-H. MÜHLHÄUSER: Max-Planck-Institut für Physik und Astrophysik, Institut für Extraterrestrische Physik, D-8046 Garching, Federal Republic of Germany

F. M. NEUBAUER: Institut für Geophysik und Meterologie der Universitat zu Köln, 5000 Köln-41, Federal Republic of Germany

V. J. PIZZO: High Altitude Observatory, National Center for Atmospheric Research, P.O. Box 3000, Boulder, CO 80307